Exp. Anim. 68(1), 103–111, 2019

—Original—

Mice harboring an MCTO mutation exhibit renal failure resembling nephropathy in human patients

Yuki TSUNAKAWA[1,2)], Michito HAMADA[1,6)], Yurina MATSUNAGA[1)], Sayaka FUSEYA[1,3)], Hyojung JEON[1)], Yuji WAKIMOTO[4)], Toshiaki USUI[1,5)], Maho KANAI[1,2)], Seiya MIZUNO[6)], Naoki MORITO[5)] and Satoru TAKAHASHI[1,6–8)]

[1)]*Department of Anatomy and Embryology, Faculty of Medicine, University of Tsukuba, 1-1-1 Tennodai, Tsukuba, Ibaraki 305-8575, Japan*
[2)]*Ph.D. Program in Human Biology, School of Integrative and Global Majors, University of Tsukuba, 1-1-1 Tennodai, Tsukuba, Ibaraki 305-8575, Japan*
[3)]*Doctoral Program in Biomedical Sciences, Graduate School of Comprehensive Human Sciences, University of Tsukuba, 1-1-1 Tennodai, Tsukuba, Ibaraki 305-8575, Japan*
[4)]*School of Medicine, Stony Brook University, Stony Brook, New York 11794, United States*
[5)]*Department of Nephrology, Faculty of Medicine, University of Tsukuba, 1-1-1 Tennodai, Tsukuba, Ibaraki 305-8575, Japan*
[6)]*Laboratory Animal Resource Center (LARC), Faculty of Medicine, University of Tsukuba, 1-1-1 Tennodai, Tsukuba, Ibaraki 305-8575, Japan*
[7)]*International Institute for Integrative Sleep Medicine (WPI-IIIS), University of Tsukuba, 1-1-1 Tennodai, Tsukuba, Ibaraki 305-8575, Japan*
[8)]*Life Science Center for Survival Dynamics, Tsukuba Advanced Research Alliance (TARA), University of Tsukuba, 1-1-1 Tennodai, Tsukuba, Ibaraki 305-8575, Japan*

Abstract: Multicentric carpotarsal osteolysis (MCTO) is a condition involving progressive osteolysis of the carpal and tarsal bones that is associated with glomerular sclerosis and renal failure (MCTO nephropathy). Previous work identified an autosomal dominant missense mutation in the transactivation domain of the transcription factor *MAFB* as the cause of MCTO. Several methods are currently used for MCTO nephropathy treatment, but these methods are invasive and lead to severe side effects, limiting their use. Therefore, the development of alternative treatments for MCTO nephropathy is required; however, the pathogenesis of MCTO *in vivo* is unclear without access to a mouse model. Here, we report the generation of an MCTO mouse model using the CRISPR/Cas9 system. These mice exhibit nephropathy symptoms that are similar to those observed in MCTO patients. *Mafb*$^{MCTO/MCTO}$ mice show developmental defects in body weight from postnatal day 0, which persist as they age. They also exhibit high urine albumin creatinine levels from a young age, mimicking the nephropathic symptoms of MCTO patients. Characteristics of glomerular sclerosis reported in human patients are also observed, such as histological evidence of focal segmental glomerulosclerosis (FSGS), podocyte foot process microvillus transformation and podocyte foot process effacement. Therefore, this study contributes to the development of an alternative treatment for MCTO nephropathy by providing a viable mouse model.

Key words: focal segmental glomerulosclerosis, MafB, multicentric carpotarsal osteolysis

(Received 2 July 2018 / Accepted 20 September 2018 / Published online in J-STAGE 26 October 2018)

Addresses corresponding: M. Hamada. e-mail: hamamichi@md.tsukuba.ac.jp
S. Takahashi. e-mail: satoruta@md.tsukuba.ac.jp

Supplementary Tables: refer to J-STAGE: https://www.jstage.jst.go.jp/browse/expanim

Introduction

Multicentric carpotarsal osteolysis (MCTO) is a rare osteolytic disease in which affected patients suffer from progressive osteolysis of the carpal and tarsal bones and may also develop renal failure in childhood [14]. Zankl *et al.* used exome capture and next-generation sequencing to reveal that an autosomal dominant missense mutation in the transactivation domain of v-maf musculoaponeurotic fibrosarcoma oncogene ortholog B (*MAFB*) causes MCTO in human patients [26].

MafB is a member of the large Maf transcription factor family, which regulates gene expression by binding as dimers to Maf recognition elements (MAREs). MafB is expressed in various cell types, such as pancreatic α and β cells; cells of the thymus, parathyroid gland, hair follicles, epidermal keratinocytes, and renal glomerulus; and cells of myeloid lineages [4, 5, 8–11, 14–16, 19, 22]. In cells of myeloid lineages, MafB has been reported to silence the self-renewal ability of macrophages and induce the expression of F4/80 to support cell differentiation [1, 17]. With regard to pathology, conditional knockout of *Mafb* in animal models specifically in hematopoietic stem cells (*Tie2-Cre::Mafb*$^{f/f}$) and myeloid cells (*LysM-Cre::Mafb*$^{f/f}$) accelerates obesity and leads to autoimmune phenotypes due to defects in the production of the complement component C1q in macrophages, respectively [23, 24]. Additionally, MafB promotes the development of atherosclerosis by inducing the expression of apoptosis inhibitor of macrophages (AIM) to prevent foam-cell apoptosis as well as excess inflammation after ischemic stroke [7, 21]. Cuevas *et al.* showed that MCTO-mutated macrophages displayed increased anti-inflammatory gene expression compared with controls, suggesting a contribution of MCTO-mutated MafB to disease progression [3].

MafB also regulates foot process development during podocyte differentiation, with *Mafb*-deficient embryos showing kidney hypoplasia and podocyte foot process effacement [17]. Fan *et al.* defined *Mafb* as a locus of susceptibility for albuminuria in the diabetic KK/Ta mice strain [6]. Morito *et al.* proved its relevance by overexpression of *Mafb* specifically in podocytes, which rescued albuminuria and nephrin depletion in mice treated with streptozotocin (STZ) [18], highlighting the importance of MafB expression in renal diseases, including MCTO. Although cyclosporine A has been successful in treating MCTO-associated nephropathy (MCTO nephropathy), patients usually suffer from side effects such as hirsutism, gingivitis, and hypertension with long-term use [2, 9]. Thus, clarification of the pathogenesis of MCTO nephropathy and the development of alternative treatments using an MCTO mouse model are needed.

The delay in producing safer treatments results from an unclear understanding of MCTO nephropathy, as insights from the use of animal models are needed. In this study, we generated a mouse harboring a human MCTO mutation c.176C>T, (p.Pro59Leu) by using the CRISPR/Cas9 system. Based on a previous analysis of *Mafb*-deficient embryos [17], we hypothesized that the MCTO missense mutation causes glomerular sclerosis via dysfunction of podocyte foot process maintenance and development.

Materials and Methods

Animals

C57BL/6J and Jcl:CD1 (ICR) mice were purchased from Charles River Laboratories Japan (Kanagawa, Japan) and CLEA Japan (Tokyo, Japan), respectively. The mice were kept in plastic cages under specific-pathogen-free conditions in a room maintained at 23.5 ± 2.5°C and 52.5 ± 12.5% relative humidity under a 14-h light:10-h dark cycle. The mice had free access to commercial chow (Milk Fat diet, Oriental Yeast, Tokyo, Japan) and filtered water. All experiments were performed in compliance with relevant Japanese and institutional laws and guidelines and were approved by the University of Tsukuba Animal Ethics Committee (authorization number 17-154).

Production of p.Pro59Leu Mafb mutant mice with CRISPR/Cas9 technology

To induce the c.176C>T mutation in the *Mafb* gene via the CRISPR/Cas9 technique, we selected the sequence 5'-GCACGGAGTGCTGAGCGGGG-3' as the guide RNA (gRNA) target. This sequence was inserted into the entry site of *pX330-U6-Chimeric_BB-CBh-hSpCas9*, which was a gift from Feng Zhang (Addgene plasmid #42230), and this plasmid was designated as *pX330-MafB*. In addition, we designed a 200-nt single-stranded DNA oligonucleotide (ssODN) donor to induce c.[176C>T;177G>T] (p.Pro59Leu) and c.174C>T (p.Thr58Thr: synonymous substitution). This synonymous substitution was designed to increase the induction efficiency of the p.Pro59Leu mutation by preventing

recutting of the edited target by active Cas9 [12]. These mutated nucleotides were placed between 98-nt 5'- and 3'-homology arms derived from positions 76–173 and 178–275 of the *Mafb* coding sequence, respectively. This MafB-P59L-ssODN was obtained from Integrated DNA Technologies (Skokie, IL, USA).

Microinjection

Pregnant mare serum gonadotropin (5 units) and human chorionic gonadotropin (5 units) were intraperitoneally injected into female C57BL/6J mice (Charles River Laboratories) with a 48-h interval between injections, and the mice were naturally mated with male C57BL/6J mice. Embryos were collected from the oviducts of the female mice, and a mixture of *pX330-MafB*(5 ng/μl) and MafB-P59L-ssODN (10 ng/μl) was injected into each male pronucleus of 292 embryos. Shortly thereafter (15 min to 2 h), 283 living embryos were transferred to the oviducts of pseudopregnant ICR mice (Charles River Laboratories, Japan), and 81 newborn mice were obtained. Of the 81 newborn mice, 6 carried the p.Pro59Leu mutation, which was confirmed by PCR with AmpliTaq Gold 360 Master Mix (Thermo Fisher Scientific, Waltham, MA, USA) and specific primers (*Mafb* mut genotype mutF, 5'-TCGGTGTCGTCCACTCTT-3'; *Mafb* mut genotype wtF, 5'-TCGGTGTCGTCCACCCCG-3'; *Mafb* mut Genotype R, 5'-CATCGTGAGTCACACCTGCT-3'). Sequencing of the PCR products was conducted using a BigDye Terminator v3.1 Cycle Sequencing Kit (Thermo Fisher Scientific, Waltham, MA, USA) and the MafB Mut Genotype F Primer (5'-ACGTCAACGACTTCGACCTT-3').

Urinary creatinine and albumin measurements

The urinary albumin and creatinine levels of the mice at specific ages were measured using a Hitachi 7170 automated analyzer (Hitachi High-Technologies Corporation, Tokyo, Japan). Albumin was determined via turbidimetric immunoassays.

Histopathological analysis of murine renal tissues

Each mouse was exsanguinated while under ether anesthesia. Its organs were then fixed with 10% formalin in 0.01 mol/l phosphate buffer (pH 7.2) and embedded in paraffin. Sections were assessed by periodic acid-Schiff (PAS) staining and Masson trichrome staining for histopathological examination under light microscopy. The ratio of sclerotic glomeruli was calculated according to a previous study [25]. In brief, PAS-stained glomeruli were counted, and sclerotic glomeruli were divided by the total number of glomeruli counted for each sample. Transmission electron microscopy was performed using standard methods.

Statistical analysis

All results are expressed as the means ± SEM. Significant differences between two groups were analyzed using Student's *t*-test. Differences were considered statistically significant at $P<0.05$.

Results

Generation of mice with the MCTO mutation with the CRISPR/Cas9 system

Zankl *et al.* reported that an autosomal dominant cystine (C) to thymine (T) missense mutation in the acidic transactivation domain of the *MAFB* gene at position 176 causes MCTO nephropathy in humans [26]. This mutation, which has also been reported by Mumm *et al.* and Mehawej *et al.*, causes both nephropathy and osteolysis in MCTO patients [14, 19]. To introduce this point mutation into the mouse genome with the CRISPR/Cas9 system, we first selected the ideal CRISPR cleavage target site within the transactivation domain of *Mafb.* As the Cas9 nuclease cleaves specific sites that are followed by a protospacer adjacent motif (PAM) sequence, we selected the site between positions 169 and 189 of the *Mafb* gene as the target sequence (Fig. 1A). We also designed a 200-nt ssODN donor for homology-directed repair (HDR)-mediated genome mutation, in which nucleotides 99, 101, and 102 from the 5' end were replaced with T. The 101st nucleotide T was placed between the 100-nt 5' and 102-nt 3' homology arms, which are equivalent to nucleotide 175 from the 5' end and nucleotide 177 from the 3' end of the *Mafb* gene, respectively. The *pX330-MafB* vector was used to express the *Mafb*-targeting gRNA under the control of the U6 promoter in zygotes. The *pX330-MafB* vector also allowed the expression of *Cas9* cDNA controlled by a *CBh* promoter, causing cleavage of the target site of *Mafb* guided by the 20-bp double-stranded DNA derived from the *Mafb* gene. The ssODN and the *pX330-MafB* vector were comicroinjected into mouse zygotes, followed by PCR analysis and sequencing analysis to screen for complete and/or mosaic pups with the MCTO mutation. Mosaic mice were further crossed with $Mafb^{WT/WT}$ mice to obtain

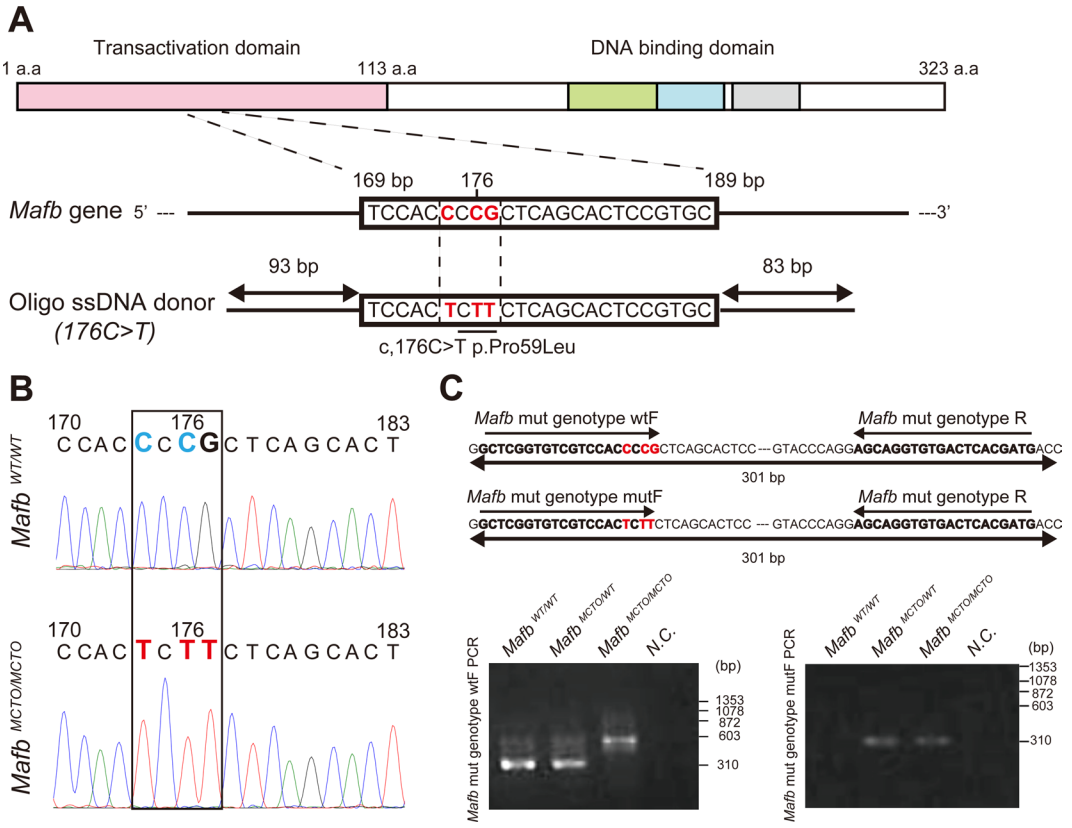

Fig. 1. *Generation of Mafb$^{MCTO/MCTO}$ mice using the CRISPR/Cas9 system.* (A) The *upper sequence* shows the *Mafb* domains within the genome. *Red box*, transactivation domain; *green box*, extended homology region; *blue box*, basic region; *gray box*, leucine zipper domain. The *middle sequence* shows the CRISPR target sequence at position 169–189 bp of the *Mafb* gene (*boxed)*. The 200-nt oligo DNA sequence is shown in the *lower sequence*. The *red bold face* C/G in the *middle sequence* and T in the *lower sequence* indicate the target nucleotide mutation. (B) Genomic sequence of the CRISPR target site in *Mafb$^{WT/WT}$* and *Mafb$^{MCTO/MCTO}$* mice. *Bold letters* in the *black box* indicate the target mutation. (C) Genotyping methods for *Mafb$^{MCTO/MCTO}$* mice. In the *upper sequence,* the *MafbWT* allele and its associated primer are illustrated (*Mafb* mut genotype wtF). The 176C>T mutation and its associated primer are shown in the *lower sequence* (*Mafb* mut genotype mutF). The genotype of each mouse was determined via PCR. Representative results of PCR are shown in the lower images.

Mafb$^{MCTO/WT}$ mice (F1 generation), and *Mafb$^{MCTO/MCTO}$* mice were obtained by crossing *Mafb$^{MCTO/WT}$* mice (F2 generation). Sequencing analysis was performed on the F2 generation to confirm the integration of the MCTO mutation (Fig. 1B), and PCR assays were performed with primer pairs for the *MafbWT* and *MafbMCTO* sequences (Fig. 1C, upper sequences). The *MafbWT* PCR product of 301 bp was observed only in *Mafb$^{WT/WT}$* and *Mafb$^{MCTO/WT}$* mice, whereas *Mafb$^{MCTO/MCTO}$* mice only exhibited a nonspecific PCR product of approximately 600 bp (Fig. 1C, lower left). A *MafbMCTO* PCR product was observed only in *Mafb$^{MCTO/WT}$* and *Mafb$^{MCTO/MCTO}$* mice, without any nonspecific PCR products (Fig. 1C, lower right).

Growth deficiency in Mafb$^{MCTO/MCTO}$ mice is observed from P0 and continues after birth

Previous reports have shown that MCTO patients exhibit nephropathy and osteolysis from early childhood [14]. To apply this finding to our *Mafb$^{MCTO/MCTO}$* mice, we examined whether *Mafb$^{MCTO/WT}$* and *Mafb$^{MCTO/MCTO}$* mice show phenotypes from postnatal day 0 (P0) to 2 weeks. At P0, *Mafb$^{MCTO/WT}$* mice showed body weights similar to *Mafb$^{MCTO/MCTO}$* mice, while *Mafb$^{MCTO/MCTO}$* mice exhibited a 10% lower body weight than *Mafb$^{WT/WT}$* mice (Fig. 2A, Table 1). The differences between *Mafb$^{WT/WT}$* and *Mafb$^{MCTO/MCTO}$* mice were still observed at 2 weeks, with *Mafb$^{MCTO/MCTO}$* mice presenting a 23% lower body weight than *Mafb$^{WT/WT}$* mice (Fig. 2B, Table

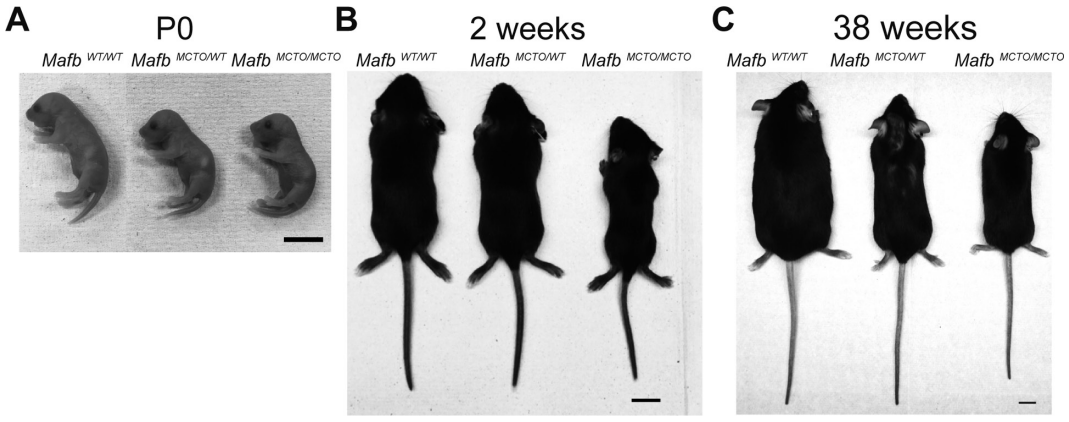

Fig. 2. *The MCTO mutation influences subsequent body growth.* (A) Representative photographs of $Mafb^{WT/WT}$, $Mafb^{MCTO/WT}$, and $Mafb^{MCTO/MCTO}$ littermates at P0. Scale bar: 1 cm. (B) Representative photographs of $Mafb^{WT/WT}$, $Mafb^{MCTO/WT}$, and $Mafb^{MCTO/MCTO}$ littermates at 2 weeks. Scale bar: 1 cm. (C) Representative photographs of $Mafb^{WT/WT}$, $Mafb^{MCTO/WT}$, and $Mafb^{MCTO/MCTO}$ littermates at 38 weeks. Scale bar: 1 cm. Table 1 provides the average weights of each genotype from P0 to 38 weeks. Supplementary Table 1, 2 and 3 provides the body weights of individual mice. The results for P0 and 2 weeks are from both male and female mice. Measurements from 2 weeks onwards were performed only in female mice. The data are presented as the mean ± SEM.; **P*<0.05 (Student's *t*-test); ***P*<0.01 (Student's *t*-test).

Table 1. Body weight of each genotype over 38 weeks

Week	$Mafb^{WT/WT}$			$Mafb^{MCTO/WT}$			$Mafb^{MCTO/MCTO}$			P value		
	Average (g)	Standard error (average ±)	Sample number	Average (g)	Standard error (average ±)	Sample number	Average (g)	Standard error (average ±)	Sample number	$Mafb^{MCTO/MCTO}$, $Mafb^{WT/WT}$	$Mafb^{MCTO/MCTO}$, $Mafb^{MCTO/WT}$	$Mafb^{MCTO/MCTO}$, $Mafb^{MCTO/MCTO}$
0 (P0)	1.41	0.04	7	1.33	0.02	10	1.29	0.49	5	0.02	0.22	0.08
2	6.96	0.54	5	6.93	0.13	10	5.40	2.41	3	0.03	0.0001	0.94
4	12.37	0.59	3	12.50	0.57	6	7.27	4.20	4	0.01	0.001	0.89
8	18.00	1.35	3	17.20	0.58	4	12.33	6.17	6	0.02	0.004	0.57
10	19.60	1.83	3	18.00	0.26	4	14.08	5.75	6	0.01	0.01	0.35
12	20.77	2.44	3	18.65	0.46	4	15.20	6.21	6	0.03	0.02	0.36
14	22.17	2.30	3	19.38	0.37	4	15.97	6.52	6	0.01	0.003	0.22
16	22.97	2.25	3	19.93	0.50	4	15.28	6.24	6	0.002	0.0003	0.18
18	23.63	1.97	3	20.18	1.01	4	16.50	7.38	5	0.02	0.03	0.24
20	24.27	1.37	6	20.60	0.50	4	17.36	5.79	9	0.0001	0.001	0.07
24	27.73	4.08	3	22.58	0.74	4	17.88	7.30	6	0.01	0.003	0.20
26	28.93	4.29	3	22.55	0.74	4	18.15	7.41	6	0.01	0.004	0.14
28	28.27	4.22	3	22.58	0.85	4	18.25	7.45	6	0.01	0.004	0.18
38	31.53	5.67	3	24.03	0.94	4	18.57	7.58	6	0.01	0.001	0.18

Note: *P* value calculated with Student's *t*-test.

1). Body weight was 40% lower in $Mafb^{MCTO/MCTO}$ mice than both $Mafb^{WT/WT}$ and $Mafb^{MCTO/WT}$ at 4 weeks (Table 1), and body weight remained lower until 38 weeks (Fig. 2C, Table 1). Although the results were not significant due to the limited sample numbers, a tendency for body weight to be lower by 24%, was observed in $Mafb^{MCTO/WT}$ mice compared with $Mafb^{WT/WT}$ mice at 38 weeks (Table 1). All the individual body weights are shown in Supplementary Table 1–3. These results indicate that the MCTO mutation not only affects development at P0 but also influences the subsequent growth pattern *in vivo*.

$Mafb^{MCTO/MCTO}$ mice exhibit an increased urine albumin creatinine ratio and develop FSGS lesions

Because renal symptoms appear in childhood in some MCTO patients with the 176C>T mutation [14], we assessed whether the $Mafb^{MCTO/MCTO}$ mice show a similar phenotype to clinical cases by analyzing the urine albumin creatinine ratio (ACR) at 4 weeks. As expected, $Mafb^{MCTO/MCTO}$ mice already exhibited urine ACR levels 6 times higher than those of $Mafb^{WT/WT}$ mice at 4 weeks, which continued until 38 weeks (Fig. 3A, Supplementary Table 4–6). Similar to body weight, 3 out of 4

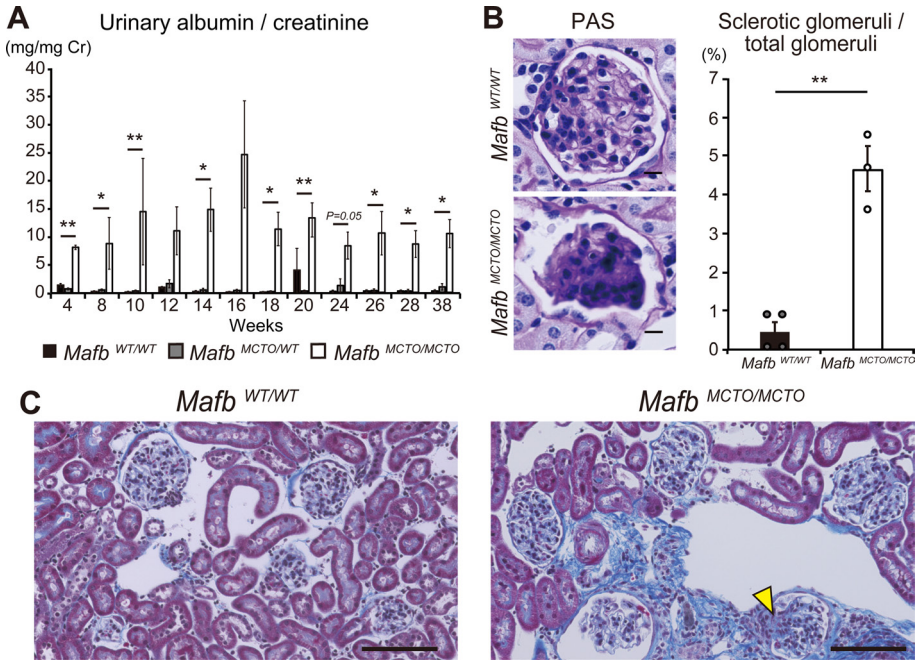

Fig. 3. *Mafb*$^{MCTO/MCTO}$ *mice exhibit an increased urine albumin creatinine ratio and FSGS phenotypes.* (A) Urinary albumin creatinine ratios measured in *Mafb*$^{WT/WT}$, *Mafb*$^{MCTO/WT}$, and *Mafb*$^{MCTO/MCTO}$ mice from 4 weeks to 38 weeks. The sample numbers of each genotype were as follows (for *Mafb*$^{WT/WT}$, *Mafb*$^{MCTOT/WT}$, and *Mafb*$^{MCTO/MCTO}$, respectively): 3, 4, and 3 at 4 weeks; 3, 4, and 4 at 8 to 12 weeks; 3, 4, and 6 at 14 to 18 weeks; 6, 4, and 9 at 20 and 26 weeks; and 3, 4, and 6 at 24, 28, and 38 weeks. Measurements at 4 weeks were performed in both male and female mice, while measurements at other times were performed only in female mice. (B) Kidneys of *Mafb*$^{WT/WT}$ and *Mafb*$^{MCTO/MCTO}$ mice subjected to PAS staining. Representative images are shown. Scale bar: 100 μm (left). The ratio of sclerotic glomeruli to total glomeruli was calculated in a blinded test (*Mafb*$^{WT/WT}$, n=4; *Mafb*$^{MCTO/MCTO}$, n=3). Solid gray circles, *Mafb*$^{WT/WT}$; solid white circles, *Mafb*$^{MCTO/MCTO}$ (right). (C) Kidneys of *Mafb*$^{WT/WT}$ and *Mafb*$^{MCTO/MCTO}$ mice stained with Masson's trichrome staining. Representative images are shown. Scale bar: 100 μm. Yellow arrowhead, sclerotic regions of a single glomerulus; blue area, fibrotic regions. Histological analyses were conducted using 25- and 26-week-old mice. Supplementary Table 4, 5, and 6 provides the urine albumin creatinine ratios of individual mice. The data are presented as the mean ± SEM.; **P*<0.05 (Student's *t*-test); ***P*<0.01 (Student's *t*-test).

samples from the *Mafb*$^{MCTO/WT}$ mice showed a trend of increased ACRs compared with *Mafb*$^{WT/WT}$ mice at 38 weeks of age (urinary albumin levels of *Mafb*$^{WT/WT}$ versus *Mafb*$^{MCTO/WT}$: 0.23, 0.24, and 0.29 versus 0.11, 0.77, 0.65, and 2.48; Fig. 3A, Supplementary Table 4–6).

Renal histopathology was also performed using PAS staining, and it was found that female *Mafb*$^{MCTO/MCTO}$ mice showed a significantly higher percentage of sclerotic glomeruli than *Mafb*$^{WT/WT}$ mice (Fig. 3B). To assess the sclerotic phenotype of *Mafb*$^{WT/WT}$ and *Mafb*$^{MCTO/MCTO}$ mice, we performed Masson's trichrome staining, which revealed that *Mafb*$^{MCTO/MCTO}$ mice showed more sclerotic glomeruli and tubulointerstitial lesions (blue regions) than *Mafb*$^{WT/WT}$ mice (Fig. 3C).

Since previous reports on *Mafb*$^{-/-}$ mice have shown podocyte foot process defects, which were also found in biopsy studies of an MCTO patient [2, 17], we performed transmission electron microscopic analysis of mature glomeruli in 25- and 26-week-old *Mafb*$^{WT/WT}$ and *Mafb*$^{MCTO/MCTO}$ female mice. Microvillous transformation of the foot processes of podocytes was frequently observed in the Bowman's space in *Mafb*$^{MCTO/MCTO}$ glomeruli, which differed from the observations for *Mafb*$^{WT/WT}$ glomeruli, and this is a known characteristic of FSGS (Fig. 4A). Higher magnification images revealed *Mafb*$^{WT/WT}$ podocytes with clear discrete foot processes, whereas *Mafb*$^{MCTO/MCTO}$ podocytes exhibited foot process effacement, similar to that seen in MCTO nephropathy

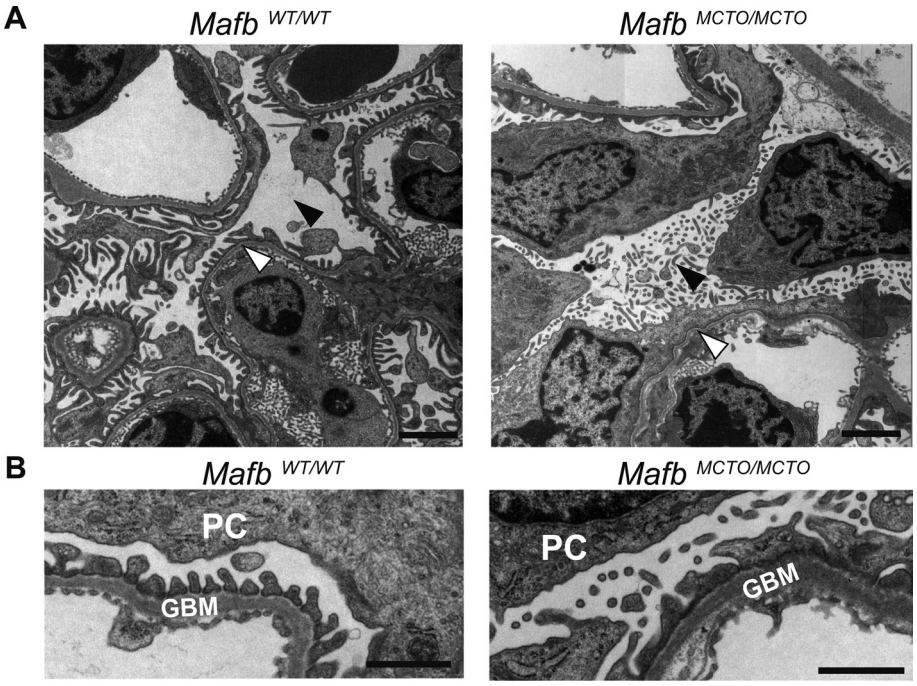

Fig. 4. *$Mafb^{MCTO/MCTO}$ mice exhibit podocyte foot process effacement and microvillous transformation*. (A) Electron microscopy image of 26-week-old female $Mafb^{WT/WT}$ and $Mafb^{MCTO/MCTO}$ glomeruli. Representative image are shown. White arrowhead, glomerular basement membrane; black arrowhead, Bowman's space; scale bar: 2 μm ($Mafb^{WT/WT}$, n=3; $Mafb^{MCTO/MCTO}$, n=3). (B) Electron microscopy images of 26-week-old female $Mafb^{WT/WT}$ and $Mafb^{MCTO/MCTO}$ podocyte foot processes at 5,000× magnification. Representative image are shown. PC, podocyte; GBM, glomerular basement membrane.

patients (Fig. 4B). Thus, $Mafb^{MCTO/MCTO}$ mice display clear evidence of podocyte defects, which resemble MCTO nephropathy symptoms, from early stages of life.

Discussion

MCTO is caused by an autosomal dominant missense mutation in the transactivation domain of the *MAFB* gene and is characterized by osteolysis of the carpal/tarsal bones and nephropathy. The development of a safer treatment for MCTO nephropathy remains a challenge because mouse model resources are limited. To overcome this issue, we generated a mouse model of MCTO via the CRISPR/Cas9 system to study the pathogenesis of MCTO nephropathy and contribute to the development of alternative treatments.

Among several mutations in *MAFB* reported to cause MCTO, we chose to generate mice with the 176C>T mutation reported by Zankl *et al.* [26]. The 176C>T mutation has been reported by several researchers, providing plausibility for comparing clinical reports and our $Mafb^{MCTO/MCTO}$ mice [14, 19]. In addition, Mehawej *et al.* reported the parental relationships of patients with the 176C>T mutation, suggesting the possibility that this mutation will be transmitted to further generations of $Mafb^{MCTO/MCTO}$ mice [14]. Moreover, since nephropathy may occur from osteolysis or vice versa, the generation of a model based on a mutation with a phenotype that includes these symptoms will provide new directions for developing treatments that take both factors into consideration.

Although MCTO nephropathy has been reported to occur from an autosomal dominant missense mutation of the *MAFB* gene [26], a milder phenotype was observed in $Mafb^{MCTO/WT}$ mice than in $Mafb^{WT/WT}$ mice. This result could be explained by previous reports on resistance against kidney defects in disease model mice with a C57BL/6J mouse background [4, 8] as well as the general differences between mice and humans [20]. Nevertheless, $Mafb^{MCTO/WT}$ mice tended to show higher ACRs than $Mafb^{WT/WT}$ mice, and this might be more evident under aged conditions. In contrast, $Mafb^{MCTO/MCTO}$ mice

showed permanently higher ACRs from 4 to 38 weeks than both *Mafb*$^{WT/WT}$ and *Mafb*$^{MCTO/WT}$ mice. Such results imitate the proteinuria observed in human patients during childhood, which arises between 0 and 6 years of age, making the *Mafb*$^{MCTO/MCTO}$ model superior to the *Mafb*$^{MCTO/WT}$ model. Histological and transmission electron microscopy analyses of the glomeruli of *Mafb*$^{MCTO/MCTO}$ mice showed evidence of FSGS and both podocyte foot process effacement and microvillous transformation. These last characteristics have both been reported in previous clinical reports on MCTO nephropathy and are typical hallmarks of FSGS, suggesting the usefulness of *Mafb*$^{MCTO/MCTO}$ mice as a model organism [2, 13, 14].

While our results indicate that *Mafb*$^{MCTO/MCTO}$ mice show MCTO nephropathic phenotypes from 4 weeks of age, the reduced body weight of *Mafb*$^{MCTO/MCTO}$ mice observed at P0 may arise as a skeletal defect, considering that symptoms also appear in the skeletal systems of MCTO patients. Therefore, further analyses are required to distinguish the tissue-specific effect of MCTO mutation in bone mineralization and remodeling. Mehawej *et al.* also reported clinical variability among patients, such as an absence of nephropathy associated with some mutations, the onset of renal symptoms associated with the same mutations, and incomplete penetrance within a family, all of which occurred for unknown reasons [14]. The generation of MCTO model mice with different mutations and further investigation of the modifier genes surrounding *MAFB* will be necessary to resolve the meaning behind these findings. Moreover, although renal failure is frequently reported in MCTO patients, diagnosis usually occurs at the later stages of the disease. Studying signs of renal failure using *Mafb*$^{MCTO/MCTO}$ mice at earlier stages may lead to the development of diagnostic measures to prevent MCTO nephropathy before chronic stages.

In conclusion, we used CRISPR/Cas9 technology to generate a mouse model of MCTO nephropathy with symptoms that resemble those of human MCTO patients. These mice showed a permanently reduced weight from birth and an excessive urine albumin creatinine ratio from an early age. Consistent with these characteristics, histological analysis showed features of podocyte defects in *Mafb*$^{MCTO/MCTO}$ mice, which may be the cause of the MCTO nephropathy. Therefore, *Mafb*$^{MCTO/MCTO}$ mice could be useful for the establishment of new treatments for MCTO nephropathy as ideal model organisms.

Acknowledgments

We especially thank Ms. Masami Ojima for her excellent technical assistance in obtaining the results. This work was supported in part by the Ministry of Education, Culture, Sports, Science and Technology (MEXT) of Japan through Grants-in-Aid for Scientific Research 26221004, 25860205, 23118504, and 16K18398. It was also supported by the Takamatsunomiya Cancer Foundation (15–24724; M. Hamada) and grants from the Uehara Memorial Foundation, Takeda Science Foundation, and World Premier International Research Center Initiative (WPI), MEXT, Japan.

References

1. Aziz, A., Soucie, E., Sarrazin, S. and Sieweke, M.H. 2009. MafB/c-Maf deficiency enables self-renewal of differentiated functional macrophages. *Science* 326: 867–871. [Medline] [CrossRef]
2. Connor, A., Highton, J., Hung, N.A., Dunbar, J., MacGinley, R. and Walker, R. 2007. Multicentric carpal-tarsal osteolysis with nephropathy treated successfully with cyclosporine A: a case report and literature review. *Am. J. Kidney Dis.* 50: 649–654. [Medline] [CrossRef]
3. Cuevas, V.D., Anta, L., Samaniego, R., Orta-Zavalza, E., Vladimir de la Rosa, J., Baujat, G., Domínguez-Soto, Á., Sánchez-Mateos, P., Escribese, M.M., Castrillo, A., Cormier-Daire, V., Vega, M.A. and Corbí, Á.L. 2017. MAFB Determines Human Macrophage Anti-Inflammatory Polarization: Relevance for the Pathogenic Mechanisms Operating in Multicentric Carpotarsal Osteolysis. *J. Immunol.* 198: 2070–2081. [Medline] [CrossRef]
4. Escano, C.S., Armando, I., Wang, X., Asico, L.D., Pascua, A., Yang, Y., Wang, Z., Lau, Y.S. and Jose, P.A. 2009. Renal dopaminergic defect in C57Bl/6J mice. *Am. J. Physiol. Regul. Integr. Comp. Physiol.* 297: R1660–R1669. [Medline] [CrossRef]
5. Eychène, A., Rocques, N. and Pouponnot, C. 2008. A new MAFia in cancer. *Nat. Rev. Cancer* 8: 683–693. [Medline] [CrossRef]
6. Fan, Q., Shike, T., Shigihara, T., Tanimoto, M., Gohda, T., Makita, Y., Wang, L.N., Horikoshi, S. and Tomino, Y. 2003. Gene expression profile in diabetic KK/Ta mice. *Kidney Int.* 64: 1978–1985. [Medline] [CrossRef]
7. Hamada, M., Nakamura, M., Tran, M.T.N., Moriguchi, T., Hong, C., Ohsumi, T., Dinh, T.T.H., Kusakabe, M., Hattori, M., Katsumata, T., Arai, S., Nakashima, K., Kudo, T., Kuroda, E., Wu, C.H., Kao, P.H., Sakai, M., Shimano, H., Miyazaki, T., Tontonoz, P. and Takahashi, S. 2014. MafB promotes atherosclerosis by inhibiting foam-cell apoptosis. *Nat. Commun.* 5: 3147. [Medline] [CrossRef]
8. Huang, L., Scarpellini, A., Funck, M., Verderio, E.A.M. and Johnson, T.S. 2013. Development of a chronic kidney disease model in C57BL/6 mice with relevance to human pa-

thology. *Nephron Extra* 3: 12–29. [Medline] [CrossRef]
9. Iijima, K., Hamahira, K., Tanaka, R., Kobayashi, A., Nozu, K., Nakamura, H. and Yoshikawa, N. 2002. Risk factors for cyclosporine-induced tubulointerstitial lesions in children with minimal change nephrotic syndrome. *Kidney Int.* 61: 1801–1805. [Medline] [CrossRef]
10. Kamitani-Kawamoto, A., Hamada, M., Moriguchi, T., Miyai, M., Saji, F., Hatamura, I., Nishikawa, K., Takayanagi, H., Hitoshi, S., Ikenaka, K., Hosoya, T., Hotta, Y., Takahashi, S. and Kataoka, K. 2011. MafB interacts with Gcm2 and regulates parathyroid hormone expression and parathyroid development. *J. Bone Miner. Res.* 26: 2463–2472. [Medline] [CrossRef]
11. Katoh, M.C., Jung, Y., Ugboma, C.M., Shimbo, M., Kuno, A., Basha, W.A., Kudo, T., Oishi, H. and Takahashi, S. 2018. MafB is critical for glucagon production and secretion in mouse pancreatic α-cells in vivo. *Mol. Cell. Biol.* 38: e00504-17. [Medline] [CrossRef]
12. Kim, H., Ishidate, T., Ghanta, K.S., Seth, M., Conte, D. Jr., Shirayama, M. and Mello, C.C. 2014. A co-CRISPR strategy for efficient genome editing in Caenorhabditis elegans. *Genetics* 197: 1069–1080. [Medline] [CrossRef]
13. Klein, C., Bellity, J., Finidori, G., Glorion, C. and Pannier, S. 2018. Multicentric carpotarsal osteolysis syndrome: long-term follow-up of three patients. *Skeletal Radiol.* 47: 1015–1019. [Medline] [CrossRef]
14. Mehawej, C., Courcet, J.B., Baujat, G., Mouy, R., Gérard, M., Landru, I., Gosselin, M., Koehrer, P., Mousson, C., Breton, S., Quartier, P., Le Merrer, M., Faivre, L. and Cormier-Daire, V. 2013. The identification of MAFB mutations in eight patients with multicentric carpo-tarsal osteolysis supports genetic homogeneity but clinical variability. *Am. J. Med. Genet. A.* 161A: 3023–3029. [Medline] [CrossRef]
15. Miyai, M., Hamada, M., Moriguchi, T., Hiruma, J., Kamitani-Kawamoto, A., Watanabe, H., Hara-Chikuma, M., Takahashi, K., Takahashi, S. and Kataoka, K. 2016. Transcription Factor MafB Coordinates Epidermal Keratinocyte Differentiation. *J. Invest. Dermatol.* 136: 1848–1857. [Medline] [CrossRef]
16. Miyai, M., Tanaka, Y.G., Kamitani, A., Hamada, M., Takahashi, S. and Kataoka, K. 2010. c-Maf and MafB transcription factors are differentially expressed in Huxley's and Henle's layers of the inner root sheath of the hair follicle and regulate cuticle formation. *J. Dermatol. Sci.* 57: 178–182. [Medline] [CrossRef]
17. Moriguchi, T., Hamada, M., Morito, N., Terunuma, T., Hasegawa, K., Zhang, C., Yokomizo, T., Esaki, R., Kuroda, E., Yoh, K., Kudo, T., Nagata, M., Greaves, D.R., Engel, J.D., Yamamoto, M. and Takahashi, S. 2006. MafB is essential for renal development and F4/80 expression in macrophages. *Mol. Cell. Biol.* 26: 5715–5727. [Medline] [CrossRef]
18. Morito, N., Yoh, K., Ojima, M., Okamura, M., Nakamura, M., Hamada, M., Shimohata, H., Moriguchi, T., Yamagata, K. and Takahashi, S. 2014. Overexpression of Mafb in podocytes protects against diabetic nephropathy. *J. Am. Soc. Nephrol.* 25: 2546–2557. [Medline] [CrossRef]
19. Mumm, S., Huskey, M., Duan, S., Wenkert, D., Madson, K.L., Gottesman, G.S., Nenninger, A.R., Laxer, R.M., McAlister, W.H. and Whyte, M.P. 2014. Multicentric carpotarsal osteolysis syndrome is caused by only a few domain-specific mutations in MAFB, a negative regulator of RANKL-induced osteoclastogenesis. *Am. J. Med. Genet. A.* 164A: 2287–2293. [Medline] [CrossRef]
20. Perlman, R.L. 2016. Mouse models of human disease: An evolutionary perspective. *Evol. Med. Public Health* 2016: 170–176. [Medline]
21. Shichita, T., Ito, M., Morita, R., Komai, K., Noguchi, Y., Ooboshi, H., Koshida, R., Takahashi, S., Kodama, T. and Yoshimura, A. 2017. MAFB prevents excess inflammation after ischemic stroke by accelerating clearance of damage signals through MSR1. *Nat. Med.* 23: 723–732. [Medline] [CrossRef]
22. Sultana, D.A., Tomita, S., Hamada, M., Iwanaga, Y., Kitahama, Y., Khang, N.V., Hirai, S., Ohigashi, I., Nitta, S., Amagai, T., Takahashi, S. and Takahama, Y. 2009. Gene expression profile of the third pharyngeal pouch reveals role of mesenchymal MafB in embryonic thymus development. *Blood* 113: 2976–2987. [Medline] [CrossRef]
23. Tran, M.T.N., Hamada, M., Jeon, H., Shiraishi, R., Asano, K., Hattori, M., Nakamura, M., Imamura, Y., Tsunakawa, Y., Fujii, R., Usui, T., Kulathunga, K., Andrea, C.S., Koshida, R., Kamei, R., Matsunaga, Y., Kobayashi, M., Oishi, H., Kudo, T. and Takahashi, S. 2017. MafB is a critical regulator of complement component C1q. *Nat. Commun.* 8: 1700. [Medline] [CrossRef]
24. Tran, M.T.N., Hamada, M., Nakamura, M., Jeon, H., Kamei, R., Tsunakawa, Y., Kulathunga, K., Lin, Y.Y., Fujisawa, K., Kudo, T. and Takahashi, S. 2016. MafB deficiency accelerates the development of obesity in mice. *FEBS Open Bio* 6: 540–547. [Medline] [CrossRef]
25. Yamamoto-Nonaka, K., Koike, M., Asanuma, K., Takagi, M., Oliva Trejo, J.A., Seki, T., Hidaka, T., Ichimura, K., Sakai, T., Tada, N., Ueno, T., Uchiyama, Y. and Tomino, Y. 2016. Cathepsin D in Podocytes Is Important in the Pathogenesis of Proteinuria and CKD. *J. Am. Soc. Nephrol.* 27: 2685–2700. [Medline]
26. Zankl, A., Duncan, E.L., Leo, P.J., Clark, G.R., Glazov, E.A., Addor, M.C., Herlin, T., Kim, C.A., Leheup, B.P., McGill, J., McTaggart, S., Mittas, S., Mitchell, A.L., Mortier, G.R., Robertson, S.P., Schroeder, M., Terhal, P. and Brown, M.A. 2012. Multicentric carpotarsal osteolysis is caused by mutations clustering in the amino-terminal transcriptional activation domain of MAFB. *Am. J. Hum. Genet.* 90: 494–501. [Medline] [CrossRef]